

# High order interpolatory Serendipity Virtual Element Method for semilinear parabolic problems.

Sergio A. Gómez<sup>a,\*</sup>

<sup>a</sup> Dipartimento di Matematica “F. Casorati”, Università di Pavia,  
Via Ferrata 5, 27100, Pavia, Italy.

---

## Abstract

We propose an efficient method for the numerical solution of a general class of two dimensional semilinear parabolic problems on polygonal meshes. The proposed approach takes advantage of the properties of the serendipity version of the Virtual Element Method (VEM), which not only significantly reduces the number of degrees of freedom compared to the classical VEM but also, under certain conditions on the mesh allows to approximate the nonlinear term with an interpolant in the Serendipity VEM space; which substantially improves the efficiency of the method. An error analysis for the semi discrete formulation is carried out, and an optimal estimate for the error in the  $L_2$ -norm is obtained. The accuracy and efficiency of the proposed method when combined with a second order Strang operator splitting time discretization is illustrated in our numerical experiments, with high order approximations up to order 6.

**Keywords:** Serendipity Virtual Element Method; Interpolatory approximation; Operator splitting method; Semilinear parabolic equations.

---

## 1. Introduction

In this work we present an interpolatory Serendipity Virtual Element Method (S-VEM) applied to a general semilinear parabolic equation on a space–time domain  $Q_T = \Omega \times (0, T)$  where  $\Omega \subset \mathbb{R}^2$  is a polygonal domain and  $T > 0$ :

$$\frac{\partial u}{\partial t} - \Delta u + f(u) = 0, \quad \text{in } Q_T, \quad (1.1a)$$

$$\nabla u \cdot \vec{n} = 0, \quad \text{on } \partial\Omega \times (0, T], \quad (1.1b)$$

$$u(\mathbf{x}, 0) = u_0(\mathbf{x}), \quad \text{in } \Omega. \quad (1.1c)$$

The model (1.1) is found in many important applications such as: battery modeling [30], crystals growth [20], population dynamics [25], and in many other models in chemistry [31, 24] and biology [22]. However, given the different nature of nonlinear terms, the task of finding exact solutions for such kind of problems becomes extremely demanding or even impossible. For that reason, there is a high interest in the development of efficient, accurate and robust numerical methods to approximate their solutions. Since this work specifically concerns to the advantages of the serendipity version of the Virtual Element Method applied to (1.1), an extensive list of numerical methods previously applied to this problem is out of our scope.

---

\*Corresponding author

Email address: [sergio.gomez01@universitadipavia.it](mailto:sergio.gomez01@universitadipavia.it) (Sergio A. Gómez)

The Virtual Element Method (VEM) is a novel technique for the numerical approximation of PDEs introduced by da Veiga *et. al.*, in [14] for an elliptic problem, and can be seen as a sensible extension of the classical finite element method to meshes with general polygonal elements. Discrete VEM spaces might contain some non-polynomial functions; however, such functions are not needed to be expressly known, since the discrete operators are directly computed from the suitably chosen degrees of freedom by means of auxiliary projections onto the space of piecewise polynomials. Besides the advantages that come from the versatility of polygonal meshes, the Virtual Element Method also allows the construction of appropriate discrete spaces without struggling to explicitly compute their basis functions.

So far the Virtual Element Method has been successfully applied to many important physical applications. In particular, recent efforts have been devoted to show the accuracy and advantages of this method in the numerical approximation of nonlinear problems such as the Cahn–Hilliard equation [8, 21], models in cardiology [7], bulk-surface reaction–diffusion systems [19], and semilinear elliptic [10, 5], hyperbolic [2] and parabolic [1] equations.

The aim of this work is to extend the idea of Adak and Natarajan in [3], where the authors proposed a VEM discretization for the sine–Gordon equation with an interpolatory approximation of the nonlinear term, thus significantly reducing the computational cost at each time step. Nevertheless, the main limitation found in [3, Sect. 7] is that their technique is only valid for approximations with  $k = 1$ , i.e., with the same order of convergence as polynomial approximations of degree  $k = 1$ ; since for  $k \geq 2$ , traditional VEM spaces require some internal (moment) degrees of freedom that unfortunately are not interpolatory. Our idea to overcome this severe limitation relies on the serendipity variation of VEM, introduced by da Veiga *et. al.*, in [16], and later discussed by Russo in [26]. The main motivation of S-VEM is indeed to eliminate internal degrees of freedom; here we use that idea to completely eliminate them. Although our approach still has some limitations, our method can compute, for instance, approximations up to  $k = 3$  for general quadrilateral meshes without suffering from distortion as it is common for serendipity FEM, see [16].

The main novelty and features of the proposed scheme are summarized as follows:

- a) To the best of our knowledge, this is the first time to use S-VEM as spatial discretization for semilinear parabolic problems.
- b) Under some restrictions on the degree  $k$ , a readily available interpolant of the nonlinear term in the S-VEM space, is introduced in the semi-discrete formulation. Such approximation significantly reduces the computational cost of evaluating the nonlinear term, avoiding the use of quadratures at each time step.
- c) Optimal error estimates in the  $L_2$ -norm are proven despite the introduction of the interpolatory approximation of the nonlinear term in the semi-discrete formulation.
- d) When the time variable is discretized by the symmetric Strang - operator splitting (SS-OS) time marching scheme, the nonlinear substeps can be decomposed as a set of completely independent one dimensional nonlinear problems.

The paper is structured as follows: in Section 2 we present the basic ideas and necessary projections for the proposed method. Optimal error estimates of order  $O(h^{k+1})$  in the  $L_2$ -norm are proven for the S-VEM approximation in Section 3. In Section 4, an efficient fully-discrete scheme, obtained from combining our interpolatory S-VEM discretization in space with a symmetric Strang - Operator Splitting time marching scheme is presented. Some numerical experiments, validating the accuracy and efficiency of the proposed method are included in Section 5. We end this work with some concluding remarks in Section 6 and some implementation details in the Appendix A.

## 2. Serendipity VEM discretization

Let  $\mathcal{T}_h$  be a partition of  $\Omega$  consisting on polygonal elements and let  $h = \max \{h_E \mid E \in \mathcal{T}_h\}$  be the mesh size, where  $h_E$  denotes the diameter of polygon  $E$ . As usual, let us first define, for each polygon  $E \in \mathcal{T}_h$ , the following enlarged local Virtual Element space [6]:

$$\tilde{V}_k(E) := \left\{ v \in C^0(\overline{E}) : v|_e \in \mathbb{P}_k(e) \quad \forall \text{ edge } e, \Delta v \in \mathbb{P}_k(E) \right\}, \quad (2.1)$$

where  $\mathbb{P}_k(e)$  and  $\mathbb{P}_k(E)$  denote the spaces of polynomials of degree at most  $k \geq 1$  on  $e$  and  $E$ , respectively.

The degrees of freedom (DOF) uniquely identifying a function  $v \in \tilde{V}_k(E)$  are choosen as:

- i) The values of  $v$  at the vertices of  $E$ .
- ii) The values of  $v$  at  $(k - 1)$  nodes on each edge  $e$  of  $E$ .
- iii) The moments  $\int_E vp_k, \forall p_k \in \mathbb{P}_k(E)$ .

A good choice for the set of degrees of freedom ii) is to take the values of any function  $v \in \tilde{V}_k(E)$  at the internal Gauss-Lobatto points on each edge. The space  $\tilde{V}_k(E)$  requires many more internal degrees of freedom than the classical VEM space, but they readily provide enough information to compute the  $L_2$ -projection of  $v$  onto  $\mathbb{P}_k(E)$ . In practice, it is not  $\tilde{V}_k(E)$  but a smaller subspace that is used as discrete space. The basic idea to construct such subspaces is to take the set of functions in  $\tilde{V}_k(E)$  sharing some moment degrees of freedom with their projection onto the space  $\mathbb{P}_k(E)$ ; which gives origin to the so called, *enhanced* [6] and *serendipity* [16] versions of VEM.

We associate to each  $E \in \mathcal{T}_h$  an integer number  $\eta_E \geq 3$ , defined as the number of distinct straight lines containing at least one edge of  $E$ . In particular, if  $E$  is an  $N$ -sides strictly convex polygon without split edges,  $\eta_E = N$ . For our purposes, we impose the following restriction on the degree of approximation:  $k < \min \{\eta_E \mid E \in \mathcal{T}_h\}$ ; which in the spirit of Serendipity VEM, allows to define a space whose associated degrees of freedom are all node evaluations at the boundaries of each polygon, without requiring any moment degree of freedom from the set iii).

The following projectors are needed to define the local S-VEM space and to present our semi-discrete formulation.

- The Ritz–Galerkin projection  $\pi_{k,E}^\nabla : \tilde{V}_k(E) \rightarrow \mathbb{P}_k(E)$  defined, for each  $v \in \tilde{V}_k(E)$  as the unique polynomial solution of:

$$\int_E \nabla(\pi_{k,E}^\nabla(v) - v) \cdot \nabla p_k d\mathbf{x} = 0, \quad \forall p_k \in \mathbb{P}_k(E), \quad (2.2a)$$

$$\int_{\partial E} \pi_{k,E}^\nabla(v) dS = \int_{\partial E} v dS, \quad (k = 1), \quad \text{or} \quad \int_E \pi_{k,E}^\nabla(v) d\mathbf{x} = \int_E v d\mathbf{x}, \quad (k > 1). \quad (2.2b)$$

Condition (2.2b) will be indistinctly denoted, for all  $k \in \mathbb{N}$ , by  $\pi_o(\pi_{k,E}^\nabla(v)) = \pi_o(v)$ . Using the Green's formula, projection  $\pi_{k,E}^\nabla(\cdot)$  can be easily computed using the degrees of freedom i), ii) and iii), see [14, Sect. 4.5].

- The standard  $L_2$ -orthogonal projector  $\pi_{k,E}^0 : \tilde{V}_k(E) \rightarrow \mathbb{P}_k(E)$ , defined as usual by

$$\int_E (\pi_{k,E}^0(v) - v) p_k d\mathbf{x} = 0, \quad \forall p_k \in \mathbb{P}_k(E), \quad (2.3)$$

is easily computable from the set of degrees of freedom iii).

- The “boundary” projector  $\pi_{k,E}^\partial : \tilde{V}_k(E) \rightarrow \mathbb{P}_k(E)$  such that

$$\int_{\partial E} (\pi_{k,E}^\partial(v) - v) p_k dS = 0, \quad \forall p_k \in \mathbb{P}_k(E), \quad (2.4)$$

is well defined under the condition  $k < \eta_E$ , and can be computed using only the boundary degrees of freedom from sets i) and ii).

We are now ready to present the local Serendipity Virtual Element space  $V_k^S(E) \subset \tilde{V}_k(E)$ , defined as:

$$V_k^S(E) = \left\{ v \in \tilde{V}_k(E) : \int_E (v - \pi_{k,E}^\partial(v)) p_k d\mathbf{x} = 0, \forall p_k \in \mathbb{P}_k(E) \right\}, \quad (2.5)$$

where clearly, for an  $N$ -sides polygon  $E$ ,  $\dim(V_k^S(E)) = Nk$ ; and the global S-VEM space is consequently defined as

$$V_k^S(\mathcal{T}_h) := \left\{ v_h \in C^0(\bar{\Omega}) : v_h|_E \in V_k^S(E), \forall E \in \mathcal{T}_h \right\}.$$

A representation of the DOF for S-VEM and the classical VEM for different  $N$ -sides polygons and the maximum degree  $k$  satisfying the aforementioned condition is presented in Fig. 1.

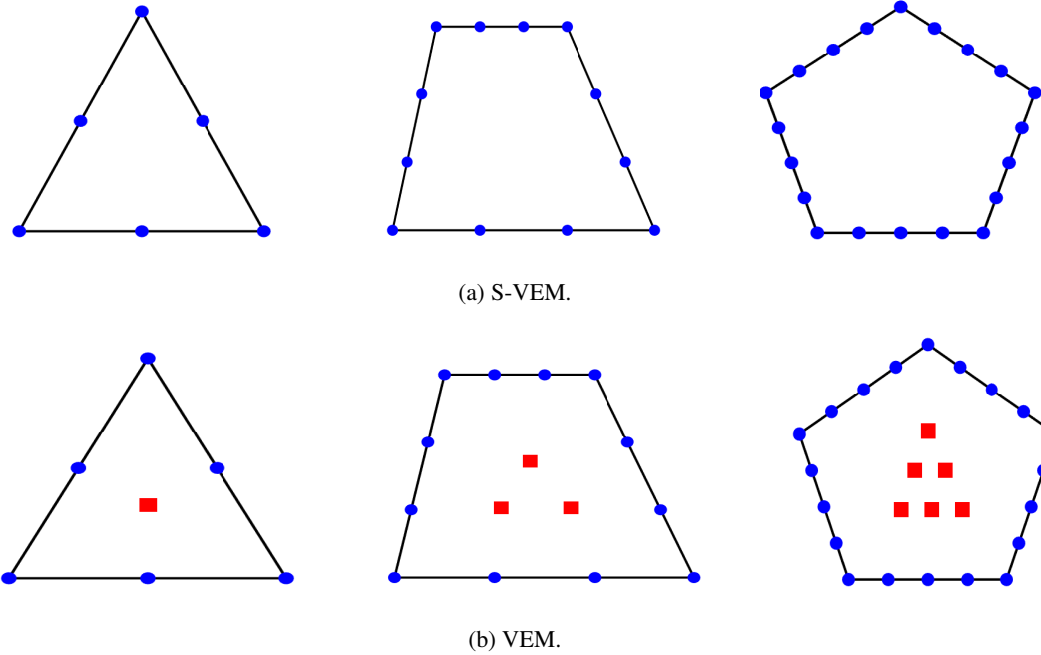


Figure 1: Degrees of freedom for two versions of VEM with degrees  $k = 2$  (triangles),  $k = 3$  (quadrilaterals), and  $k = 4$  (pentagons). Blue dots represent node evaluations, and red squares represent internal moments.

Let us notice that, since the moments up to degree  $k$  of any  $v \in V_k^S(E)$  coincide with those of  $\pi_{k,E}^\partial(v)$ , it is evident that

$$\pi_{k,E}^0(v) = \pi_{k,E}^\partial(v), \quad \forall v \in V_k^S(E); \quad (2.6)$$

and under this premise we will make no distinction between them from now on.

As mentioned before, a function  $v \in V_k^S(E)$  is uniquely determined by its boundary degrees of freedom. Denoting by  $d_{k,E}^S = \dim(V_k^S(E))$ , and numbering the nodes associated to the chosen degrees of freedom as  $\xi_i$ , with  $i = 1, \dots, d_{k,E}^S$ , we can define the functions  $\text{dof}_i : V_k^S(E) \rightarrow \mathbb{R}$  as

$$\text{dof}_i(v) := v(\xi_i), \quad \forall v \in V_k^S(E),$$

and a natural basis arise, by taking the canonical basis functions  $\{\phi_i\}_{i=1}^{d_{k,E}^S}$  satisfying

$$\text{dof}_i(\phi_j) = \delta_{ij}, \quad i, j = 1, \dots, d_{k,E}^S. \quad (2.7)$$

The following interpolatory representation is obtained for all  $v \in V_k^S(E)$ :

$$v(\mathbf{x}) = \sum_{i=1}^{d_{k,E}^S} \text{dof}_i(v) \phi_i(\mathbf{x}) = \sum_{i=1}^{d_{k,E}^S} v(\xi_i) \phi_i(\mathbf{x}); \quad (2.8)$$

such representation in turn allows us to define the interpolatory operator  $\mathcal{I}_h^k : C^0(\overline{\Omega}) \rightarrow V_k^S(\mathcal{T}_h)$  whose restriction to each polygon  $E \in \mathcal{T}_h$  is given by:

$$\mathcal{I}_h^{k,E} g(\mathbf{x}) := \sum_{i=1}^{d_{k,E}^S} g(\xi_i) \phi_i(\mathbf{x}). \quad (2.9)$$

### 2.1. Semi-discrete formulation

The weak formulation of the model problem (1.1) is: find  $u \in L_2(0, T, H^1(\Omega))$  with  $u_t \in L_2(0, T, H^{-1}(\Omega))$  such that

$$\left( \frac{\partial u}{\partial t}; v \right)_\Omega + a(u; v) + (f(u); v)_\Omega = 0, \quad \forall v \in H^1(\Omega), \quad (2.10)$$

where  $(\cdot; \cdot)_\Omega : L_2(\Omega) \times L_2(\Omega) \rightarrow \mathbb{R}$  and  $a(\cdot; \cdot) : H^1(\Omega) \times H^1(\Omega) \rightarrow \mathbb{R}$  are the bilinear forms defined as

$$(u; v)_\Omega := \int_\Omega u v d\mathbf{x}, \quad a(u; v) := \int_\Omega \nabla u \cdot \nabla v d\mathbf{x}.$$

Analogously, our semi-discrete interpolatory S-VEM formulation seeks an approximation  $u_h \in V_k^S(\mathcal{T}_h)$  such that for all test functions  $v_h \in V_k^S(\mathcal{T}_h)$  it satisfies

$$m_h \left( \frac{\partial u_h}{\partial t}; v_h \right) + a_h(u_h; v_h) + m_h(\mathcal{I}_h^k f(u_h); v_h) = 0, \quad (2.11a)$$

$$u_h^0 = \mathcal{I}_h^k u_0, \quad (2.11b)$$

where the bilinear forms  $a_h : V_k^S(\mathcal{T}_h) \times V_k^S(\mathcal{T}_h) \rightarrow \mathbb{R}$  and  $m_h : V_k^S(\mathcal{T}_h) \times V_k^S(\mathcal{T}_h) \rightarrow \mathbb{R}$  are locally constructed as

$$a_h(u_h; v_h) = \sum_{E \in \mathcal{T}_h} a_h^E(u_h; v_h), \quad m_h(u_h; v_h) = \sum_{E \in \mathcal{T}_h} m_h^E(u_h; v_h),$$

and the restrictions  $a_h^E(\cdot; \cdot)$  and  $m_h^E(\cdot; \cdot)$  are split into a consistency and a stability terms by

$$a_h^E(u_h; v_h) = a^E(\pi_{k,E}^\nabla(u_h); \pi_{k,E}^\nabla(v_h)) + s_a^E((I - \pi_{k,E}^\nabla)u_h; (I - \pi_{k,E}^\nabla)v_h), \quad (2.12a)$$

$$m_h^E(u_h; v_h) = m^E(\pi_{k,E}^\partial(u_h); \pi_{k,E}^\partial(v_h)) + s_m^E((I - \pi_{k,E}^\partial)u_h; (I - \pi_{k,E}^\partial)v_h), \quad (2.12b)$$

where  $m^E(u; v) := (u; v)_E$ ; and the stabilization terms  $s_a^E(\cdot; \cdot)$ ,  $s_m^E(\cdot; \cdot)$  are symmetric bilinear forms scaling as  $a^E(\cdot; \cdot)$  and  $m^E(\cdot; \cdot)$ , respectively; more precisely, there exist positive constants  $\alpha_1, \alpha_2, \beta_1, \beta_2$  such that the following inequalities hold

$$\alpha_1 a^E(v_h; v_h) \leq s_a^E(v_h; v_h) \leq \alpha_2 a^E(v_h; v_h), \quad \forall v_h \in V_k^S(E) \cap \text{Ker}(\pi_k^\nabla), \quad (2.13a)$$

$$\beta_1 m^E(v_h; v_h) \leq s_m^E(v_h; v_h) \leq \beta_2 m^E(v_h; v_h), \quad \forall v_h \in V_k^S(E) \cap \text{Ker}(\pi_k^\partial). \quad (2.13b)$$

In fact, there are many possible choices for the stability terms; however, we will limit ourselves to use a very simple stabilization proposed in [14]. For a thorough study on different stability choices, see [17, 23]. By construction, both  $a_h(\cdot; \cdot)$  and  $m_h(\cdot; \cdot)$  satisfy the following two important conditions:

- **k-Polynomial consistency:** For all  $E \in \mathcal{T}_h$  we have

$$a_h^E(p_k; v_h) = a^E(p_k; v_h), \quad \forall p \in \mathbb{P}_k(E), \quad \forall v_h \in V_k^S(E), \quad (2.14a)$$

$$m_h^E(p_k; v_h) = m^E(p_k; v_h), \quad \forall p \in \mathbb{P}_k(E), \quad \forall v_h \in V_k^S(E). \quad (2.14b)$$

- **Stability:** There exist mesh-independent constants  $\alpha_*, \alpha^*, \beta_*, \beta^*$  such that

$$\alpha_* a^E(v_h; v_h) \leq a_h^E(v_h; v_h) \leq \alpha^* a^E(v_h; v_h), \quad \forall v_h \in V_k^S(E), \quad (2.15a)$$

$$\beta_* m^E(v_h; v_h) \leq m_h^E(v_h; v_h) \leq \beta^* m^E(v_h; v_h), \quad \forall v_h \in V_k^S(E). \quad (2.15b)$$

Let us highlight that the last term in (2.11a) satisfies the following identity:

$$\begin{aligned} m_h(\mathcal{I}_h^k f(u_h); \phi_i) &= \sum_{E \in \mathcal{T}_h} m_h^E(\mathcal{I}_h^k f(u_h); \phi_i) \stackrel{(2.8)}{=} \sum_{E \in \mathcal{T}_h} \sum_{j=1}^{d_{k,E}^S} \text{dof}_j(f(u_h)) m_h^E(\phi_i; \phi_j) \\ &\stackrel{(2.9)}{=} \sum_{E \in \mathcal{T}_h} \sum_{j=1}^{d_{k,E}^S} f(u_h(\xi_j)) m_h^E(\phi_i; \phi_j) \\ &\stackrel{(2.8)}{=} \sum_{E \in \mathcal{T}_h} \sum_{j=1}^{d_{k,E}^S} f(\text{dof}_j(u_h)) m_h^E(\phi_i; \phi_j), \end{aligned} \quad (2.16)$$

which clearly shows that the evaluation of the nonlinear term only requires to compute the matrix representation of  $m_h(\cdot; \cdot)$  and the evaluation of  $f(\cdot)$  at the degrees of freedom of  $u_h$ .

**Remark 1.** *Applying stabilization in the last term of (2.11a) is not necessary to obtain optimal convergence, but it can be computationally convenient as shown in Section 4. In fact, we can justify such term by considering the following integral*

$$\begin{aligned} (\mathcal{I}_h^k f(u_h); \phi_i)_\Omega &= \sum_{E \in \mathcal{T}_h} \sum_{j=1}^{d_{k,E}^S} f(u_h(\xi_j)) (\phi_i; \phi_j)_E \\ &= \sum_{E \in \mathcal{T}_h} \sum_{j=1}^{d_{k,E}^S} f(u_h(\xi_j)) \left[ (\pi_{k,E}^\partial(\phi_i); \pi_{k,E}^\partial(\phi_j))_E + ((I - \pi_k^\partial)\phi_i; (I - \pi_k^\partial)\phi_j)_E \right] \end{aligned}$$

$$+ \left( \pi_{k,E}^\partial(\phi_i); (I - \pi_{k,E}^\partial)\phi_j \right)_E + \left( (I - \pi_{k,E}^\partial)\phi_i; \pi_{k,E}^\partial(\phi_j) \right)_E \Bigg],$$

and remembering that  $\pi_{k,E}^\partial(v_h) = \pi_{k,E}^0(v_h)$ ,  $\forall v_h \in V_k^S(E)$ . By definition of  $\pi_{k,E}^\partial$  the last two terms vanish and the remaining two terms are indeed the original motivation for the consistency and stability parts of  $m_h^E(\cdot; \cdot)$ .

**Remark 2.** The initial condition approximation  $u_h^0 = \mathcal{I}_h^k u_0$  in (2.11b) could be replaced by  $u_h^0 = \pi_k^0(u_0)$ ; however, the choice in (2.11b) is suitable for imposing random initial data, which is commonly of interest in this kind of problems.

### 3. Error analysis

This section is devoted to get an optimal error estimate in the  $L_2$ -norm for the solution of the semi-discrete formulation (2.11). The main ideas are taken from the error analysis carried out in [32] for the classical VEM applied to linear parabolic problems and its recent extensions to semilinear parabolic problems [5, 1, 4]. Nonetheless, in Theorem 1 we address the following differences:

- The approximated solution belongs to  $V_k^S(\mathcal{T}_h)$  instead of the enhanced VEM space  $W_k(\mathcal{T}_h) \subset V_k(\mathcal{T}_h)$ , whose elements only share the same moments of degree  $(k-1)$  and  $k$  as the projection  $\pi_k^\nabla(\cdot)$ , see [6] for details.
- The nonlinear term is approximated by its interpolant  $\mathcal{I}_h^k f(u_h) \in V_k^S(\mathcal{T}_h)$ ; and in our semi-discrete formulation (2.11) we use  $m_h(\mathcal{I}_h^k f(u_h); v_h)$  in place of the term  $m_h(\pi_k^0(\mathcal{I}_h^k f(u_h)); v_h)$  used by Adak and Natarajan in [3] for the sine-Gordon equation.
- Pure homogeneous Neumann boundary conditions are considered.

In what follows we will make the following assumptions on the mesh, the degree parameter  $k$  and the nonlinear function  $f(\cdot)$ :

**Assumption 1.** Every  $E \in \mathcal{T}_h$  is an open and bounded polygon, with diameter  $h_E$ , star-shaped with respect to the ball  $B := B_{\rho h_E}(z)$  centered at  $z \in E$  and with radius  $\rho h_E$ , for some  $0 < \rho \leq 1$ .

**Assumption 2.** The parameter  $k$  in the definition of  $V_k^S(\mathcal{T}_h)$  satisfies the restriction  $k < \min\{\eta_E : E \in \mathcal{T}_h\}$ .

**Assumption 3.** The nonlinear function  $f : \mathbb{R} \rightarrow \mathbb{R}$  is globally Lipschitz continuous, i.e., there exists a constant  $L_f > 0$  such that the following inequality holds:

$$|f(x) - f(y)| \leq L_f |x - y|, \quad \forall x, y \in \mathbb{R}. \quad (3.1)$$

For  $k \in \mathbb{N}$  satisfying Assumption 2, the elliptic projection operator  $\mathcal{P}_h : H^1(\Omega) \rightarrow V_k^S(\mathcal{T}_h)$ , is defined for each function  $u \in H^1(\Omega)$  as the only element  $\mathcal{P}_h(u) \in V_k^S(\mathcal{T}_h)$  satisfying:

$$\begin{cases} a_h(\mathcal{P}_h(u); v_h) = a(u; v_h), & \forall v_h \in V_k^S(\mathcal{T}_h), \\ \int_{\Omega} \mathcal{P}_h(u) dx = 0. \end{cases} \quad (3.2)$$

Since  $\mathcal{P}_h(u)$  is the solution of the variational problem (3.2), by the coercivity and continuity of  $a_h(\cdot; \cdot)$  and the continuity of the linear functional  $a(u; \cdot)$ , the projection operator  $\mathcal{P}_h$  is well defined. Furthermore, we can prove the following estimate as in [32, Lemma 3.1].

**Lemma 1.** Let  $\Omega$  be a convex domain, and  $u \in H^{k+1}(\Omega)$ . Under Assumptions 1 and 2, there exists a positive constant  $C_\alpha > 0$ , depending on  $\alpha_*$  and  $\alpha^*$  in (2.15a) but independent on  $h$  such that:

$$\|\mathcal{P}_h(u) - u\|_{L_2(\Omega)} \leq C_\alpha h^{k+1} |u|_{H^{k+1}(\Omega)}. \quad (3.3)$$

Using standard arguments as in [14] and the classical Dupont-Scott theory in [9], the following estimates for the interpolant  $\mathcal{I}_h^k(\cdot)$  and the projections  $\pi_k^\partial(\cdot), \pi_k^\nabla(\cdot)$  are obtained.

**Lemma 2.** Under Assumptions 1 and 2. If  $u \in H^{k+1}(\Omega)$ , there exists a constant  $C_I$ , depending only on  $k$  and  $\rho$ , such that the interpolant  $\mathcal{I}_h^k u \in V_k^S(\mathcal{T}_h)$  satisfies:

$$\|u - \mathcal{I}_h^k u\|_{L_2(E)} + h |u - \mathcal{I}_h^k u|_{H^1(E)} \leq C_I h^{k+1} |u|_{H^{k+1}(E)}, \quad \forall E \in \mathcal{T}_h. \quad (3.4)$$

**Lemma 3.** Under Assumptions 1 and 2. For each  $E \in \mathcal{T}_h$ , if  $u \in H^{k+1}(E)$ , there exists a polynomial  $u_\pi \in \mathbb{P}_k(E)$ , and a positive constant  $C_\pi > 0$ , depending only on  $k$  and  $\rho$ , such that:

$$\|u - u_\pi\|_{L_2(E)} + h |u - u_\pi|_{H^1(E)} \leq C_\pi h^{k+1} |u|_{H^{k+1}(E)}, \quad (3.5)$$

which implies optimal convergence for the  $L_2$ -projection operator  $\pi_k^0(u)$  and as such, by (2.6), for the projection  $\pi_k^\partial(u)$ .

The following theorem, provides the optimal error estimate for the semi-discrete formulation (2.11) under suitable regularity conditions for the exact solution. We will use  $C$  to denote a generic constant independent of the mesh size  $h$ ; and the arguments of the functions in the proof will be omitted unless they are necessary.

**Theorem 1.** Under Assumptions 1–3. Let  $\Omega$  be a convex domain, and  $u$  and  $u_h$  be the solutions of the variational problems (2.10) and (2.11), respectively. For  $u$  and  $f(u)$  smooth enough, there exists a positive constant  $C$  independent of  $h$ , such that for all  $t \in (0, T]$  the following bound holds:

$$\begin{aligned} \|u_h(\cdot, t) - u(\cdot, t)\|_{L_2(\Omega)} &\leq Ch^{k+1} \left( |u_0|_{H^{k+1}(\Omega)} + \|u_t\|_{L_1(0, t, H^{k+1}(\Omega))} + \|u\|_{L_2(0, t, H^{k+1}(\Omega))} \right. \\ &\quad \left. + \|f(u)\|_{L_2(0, t, H^{k+1}(\Omega))} + \|\mathcal{I}_h^k f(u)\|_{L_2(0, t, H^{k+1}(\Omega))} \right) \end{aligned} \quad (3.6)$$

*Proof.*

We start decomposing  $e_u := u - u_h$  as  $e_u = \xi_u - \theta_h$ , where  $\xi_u = u - \mathcal{P}_h(u)$  and  $\theta_h = u_h - \mathcal{P}_h(u)$ . From Lemma 1 and the identity  $u(\cdot, t) = u(\cdot, 0) + \int_0^t u_t(\cdot, s)ds$  we have the following bound for  $\xi_u$ :

$$\|\xi_u(\cdot, t)\|_{L_2(\Omega)} \leq Ch^{k+1} \left( |u_0|_{H^{k+1}(\Omega)} + |u_t|_{L_1(0, t, H^{k+1}(\Omega))} \right). \quad (3.7)$$

Therefore, in order to get the desired estimate, it only remains to bound  $\|\theta_h(\cdot, t)\|_{L_2(\Omega)}$ . We now proceed similarly as in [1]; since  $\theta_h \in V_k^S(\mathcal{T}_h)$ , adding and subtracting appropriate terms in the semi discrete formulation (2.11a), for any  $v_h \in V_k^S(\mathcal{T}_h)$  we get

$$\begin{aligned} m_h \left( \frac{\partial \theta_h}{\partial t}; v_h \right) + a_h(\theta_h; v_h) &= -m_h \left( \mathcal{I}_h^k f(u_h); v_h \right) - m_h \left( \frac{\partial}{\partial t} \mathcal{P}_h(u); v_h \right) - a_h(\mathcal{P}_h(u); v_h) \\ &\stackrel{(3.2)}{=} -m_h \left( \mathcal{I}_h^k f(u_h); v_h \right) - m_h \left( \frac{\partial}{\partial t} \mathcal{P}_h(u); v_h \right) - a(u; v_h) \end{aligned}$$

$$\begin{aligned}
& \stackrel{(2.10)}{=} (f(u); v_h)_\Omega - m_h \left( \mathcal{I}_h^k f(u_h); v_h \right) + \left( \frac{\partial u}{\partial t}; v_h \right)_\Omega - m_h \left( \frac{\partial}{\partial t} \mathcal{P}_h(u); v_h \right) \\
& \stackrel{(2.12b)}{=} \sum_{E \in \mathcal{T}_h} \left[ \underbrace{m^E(f(u); v_h) - m_h^E(\mathcal{I}_h^k f(u_h); v_h)}_{T_1^E} + \underbrace{m^E\left(\frac{\partial u}{\partial t}; v_h\right) - m_h^E\left(\frac{\partial}{\partial t} \mathcal{P}_h(u); v_h\right)}_{T_2^E} \right], \tag{3.8}
\end{aligned}$$

hence, we will look for local estimates for  $T_1^E$  and  $T_2^E$  on each  $E \in \mathcal{T}_h$ .

By the  $k$ -polynomial consistency property (2.14b) of  $m_h(\cdot; \cdot)$ , we can decompose  $T_1^E$  as:

$$\begin{aligned}
m^E(f(u); v_h) - m_h^E(\mathcal{I}_h^k f(u_h); v_h) & \stackrel{(2.14b)}{=} m^E(f(u) - \pi_k^0(f(u)); v_h) + m^E(\pi_k^0(f(u)) - \pi_k^0(\mathcal{I}_h^k f(u)); v_h) \\
& \quad + m_h^E(\pi_k^0(\mathcal{I}_h^k f(u)) - \mathcal{I}_h^k f(u_h); v_h) \\
& = R_1 + R_2 + R_3. \tag{3.9}
\end{aligned}$$

By Cauchy-Schwarz inequality and Lemma 3, it is easy to see that

$$|R_1| \stackrel{(3.5)}{\leq} C_\pi h^{k+1} |f(u)|_{H^{k+1}(E)} \|v_h\|_{L_2(E)}. \tag{3.10}$$

On the other hand, by the boundedness of the  $L_2$ -projection operator  $\pi_k^0(\cdot)$  and Lemma 2 we have:

$$|R_2| \leq \|f(u) - \mathcal{I}_h^k f(u)\|_{L_2(E)} \|v_h\|_{L_2(E)} \stackrel{(3.4)}{\leq} C h^{k+1} |f(u)|_{H^{k+1}(E)} \|v_h\|_{L_2(E)}. \tag{3.11}$$

To bound  $R_3$ , we first observe that:

$$\begin{aligned}
\|\mathcal{I}_h^k f(u) - \mathcal{I}_h^k f(u_h)\|_{L_2(E)}^2 & = \int_E |\mathcal{I}_h^k(f(u) - f(u_h))|^2 d\mathbf{x} \stackrel{(2.9)}{=} \int_E \left| \sum_{i=1}^{d_{k,E}^S} (f(u(\xi_i)) - f(u_h(\xi_i))) \phi_i \right|^2 d\mathbf{x} \\
& \stackrel{(3.1)}{\leq} L_f^2 \int_E \left| \sum_{i=1}^{d_{k,E}^S} (u(\xi_i) - u_h(\xi_i)) \phi_i \right|^2 d\mathbf{x} \\
& = L_f^2 \|\mathcal{I}_h^k u - u_h\|_{L_2(E)}^2 \tag{3.12}
\end{aligned}$$

therefore  $\|\mathcal{I}_h^k f(u) - \mathcal{I}_h^k f(u_h)\|_{L_2(E)} \leq L_f \|\mathcal{I}_h^k u - u_h\|_{L_2(E)}$ ; and together with triangle's inequality and the continuity of  $m_h(\cdot; \cdot)$  it provides the following bound for  $R_3$ :

$$\begin{aligned}
|R_3| & \stackrel{(2.15b)}{\leq} \beta^* \|\pi_k^0(\mathcal{I}_h^k f(u)) - \mathcal{I}_h^k f(u_h)\|_{L_2(E)} \|v_h\|_{L_2(E)} \\
& \leq \beta^* \left( \|\pi_k^0(\mathcal{I}_h^k f(u)) - \mathcal{I}_h^k f(u)\|_{L_2(E)} + \|\mathcal{I}_h^k f(u) - \mathcal{I}_h^k f(u_h)\|_{L_2(E)} \right) \|v_h\|_{L_2(E)} \\
& \stackrel{(3.12)}{\leq} \beta^* \left( C_\pi h^{k+1} |\mathcal{I}_h^k f(u)|_{H^{k+1}(E)} + L_f \|\mathcal{I}_h^k u - u_h\|_{L_2(E)} \right) \|v_h\|_{L_2(E)} \\
& \leq \beta^* \left( C_\pi h^{k+1} |\mathcal{I}_h^k f(u)|_{H^{k+1}(E)} + L_f \|\mathcal{I}_h^k u - u\|_{L_2(E)} + L_f \|e_u\|_{L_2(E)} \right) \|v_h\|_{L_2(E)} \\
& \leq C \left( h^{k+1} |\mathcal{I}_h^k f(u)|_{H^{k+1}(E)} + h^{k+1} |u|_{H^{k+1}(E)} + \|e_u\|_{L_2(E)} \right) \|v_h\|_{L_2(E)}. \tag{3.13}
\end{aligned}$$

In a similar way, decomposing

$$m^E(u_t; v_h) - m_h^E(\mathcal{P}_h(u_t); v_h) = m^E(u_t - \pi_k^0(u_t); v_h) - m_h^E(\mathcal{P}_h(u_t) - \pi_k^0(u_t); v_h),$$

and applying similar steps as before, by the commutativity of  $\frac{\partial}{\partial t}(\cdot)$  and  $\mathcal{P}_h(\cdot)$  we get the following bound for  $T_2^E$

$$|T_2^E| \leq Ch^{k+1} |u_t|_{H^{k+1}(E)}. \quad (3.14)$$

Integrating from 0 to  $t$  at both sides of (3.8) for  $v_h = \theta_h$ ; since  $a_h(\theta_h; \theta_h) \geq 0$ , by the estimate (3.7) for  $\xi_u$ , the bounds (3.10)–(3.14) and Young's inequality we get the following estimate

$$\begin{aligned} \|\theta_h(\cdot, t)\|_{L_2(\Omega)}^2 &\stackrel{(2.15b)}{\leq} \beta_*^{-1} m_h(\theta_h(\cdot, t); \theta_h(\cdot, t)) + 2\beta_*^{-1} \int_0^t a_h(\theta_h; \theta_h) ds \\ &\leq C m_h(\theta_h(\cdot, 0); \theta_h(\cdot, 0)) + C \int_0^t \|e_u\|_{L_2(\Omega)} \|\theta_h\|_{L_2(\Omega)} ds \\ &\quad + Ch^{k+1} \int_0^t \left( |f(u)|_{H^{k+1}(\Omega)} + |\mathcal{I}_h^k f(u)|_{H^{k+1}(\Omega)} + |u|_{H^{k+1}(\Omega)} + |u_t|_{H^{k+1}(\Omega)} \right) \|\theta_h\|_{L_2(\Omega)} ds \\ &\leq C m_h(\theta_h(\cdot, 0); \theta_h(\cdot, 0)) + C \int_0^t \left( \|\xi_u\|_{L_2(\Omega)} \|\theta_h\|_{L_2(\Omega)} + \|\theta_h\|_{L_2(\Omega)}^2 \right) ds \\ &\quad + Ch^{k+1} \int_0^t \left( |f(u)|_{H^{k+1}(\Omega)} + |\mathcal{I}_h^k f(u)|_{H^{k+1}(\Omega)} + |u|_{H^{k+1}(\Omega)} + |u_t|_{H^{k+1}(\Omega)} \right) \|\theta_h\|_{L_2(\Omega)} ds \\ &\stackrel{(3.7)}{\leq} C m_h(\theta_h(\cdot, 0); \theta_h(\cdot, 0)) + \int_0^t C \|\theta_h(\cdot, s)\|_{L_2(\Omega)}^2 ds + Ch^{k+1} \left( |u_0|_{H^{k+1}(\Omega)}^2 + \|u_t\|_{L_1(0,t,H^{k+1}(\Omega))}^2 \right. \\ &\quad \left. + \|u\|_{L_2(0,t,H^{k+1}(\Omega))}^2 + \|f(u)\|_{L_2(0,t,H^{k+1}(\Omega))}^2 + \|\mathcal{I}_h^k f(u)\|_{L_2(0,t,H^{k+1}(\Omega))}^2 \right), \end{aligned}$$

and by Grönwall's lemma, since  $\theta_h(\cdot, 0) = (\mathcal{P}_h(u_0) - u_0) + (u_0 - \mathcal{I}_h^k u_0)$ , combined with the bound (3.7) for  $\xi_u$ , and the estimates (3.3)–(3.4), we get the desired estimate (3.6) in our Theorem.  $\square$

**Remark 3.** If we replace  $m_h(\mathcal{I}_h^k f(u_h); v_h)$  in the semi-discrete formulation (2.11) by  $m_h(\pi_k^0(\mathcal{I}_h^k f(u_h)); v_h)$ , the term  $\|\mathcal{I}_h^k f(u)\|_{L_2(0,t,H^{k+1}(\Omega))}$  in the estimate (3.6) can be easily removed.

#### 4. Fully discrete scheme

Denoting by  $M$  and  $A$  the matrix representation of the bilinear forms  $m_h(\cdot; \cdot)$  and  $a_h(\cdot; \cdot)$ , respectively; by the identity (2.16), the semi-discrete formulation (2.11) can be written as a system of nonlinear differential equations as

$$M \frac{dU_h}{dt} + AU_h + Mf(U_h) = 0, \quad (4.1)$$

where  $U_h$  is the vector of the representation coefficients of  $u_h$  in the basis of  $V_k^S(\mathcal{T}_h)$ ; and  $f(U_h)$  is simply the vector of component-wise evaluation of function  $f(\cdot)$  at  $U_h$ .

Even though we expect that the efficiency of any ODE solver applied to (4.1) will be greatly benefited from the easy evaluation of the nonlinear term, in this paper we choose the second order symmetric Strang operator splitting (SS-OS) method [29] as time marching scheme; which decomposes the system of

differential equations (4.1) as a series of linear and nonlinear substeps, usually associated to diffusion and reaction terms, of the form

$$U_h^{(1)} = \mathcal{D}_{\tau/2}(U_h^n), \quad U_h^{(2)} = \mathcal{R}_\tau(U_h^{(1)}), \quad U_h^{n+1} = \mathcal{D}_{\tau/2}(U_h^{(2)}), \quad (4.2a)$$

$$\text{or} \quad U_h^{(1)} = \mathcal{R}_{\tau/2}(U_h^n), \quad U_h^{(2)} = \mathcal{D}_\tau(U_h^{(1)}), \quad U_h^{n+1} = \mathcal{R}_{\tau/2}(U_h^{(2)}), \quad (4.2b)$$

where  $\tau = t_{n+1} - t_n$  and  $U_h^n$  is the vector approximation of  $u_h(\cdot, t_n)$ .

The efficiency of combining some discontinuous Galerkin methods with an interpolatory approximation of the nonlinear term as spatial discretization on classical meshes and the SS-OS time marching scheme was assessed by Castillo and Gómez in [12, 13].

A necessary condition to retain the second order accuracy of the full SS-OS step is that each substep in (4.2) must be solved with a second order ODE solver itself. Despite the freedom we have to choose each solver, implicit methods might be more appropriate; on the contrary, in the linear substeps we could face a very restrictive CFL condition, while for the nonlinear substeps the method might become unstable in the case of stiff nonlinear term.

From the discussion above we decide to apply the Crank-Nicolson method to each substep in (4.2). For the  $\mathcal{DRD}$  decomposition (4.2a) the resulting fully discrete method reads

$$\left(M + \frac{\tau}{4}A\right)U_h^{(1)} = \left(M - \frac{\tau}{4}A\right)U_h^n, \quad (4.3a)$$

$$U_h^{(2)} = U_h^{(1)} - \frac{\tau}{2}(f(U_h^{(1)}) + f(U_h^{(2)})), \quad (4.3b)$$

$$\left(M + \frac{\tau}{4}A\right)U_h^{n+1} = \left(M - \frac{\tau}{4}A\right)U_h^{(2)}. \quad (4.3c)$$

The following remarks are in order:

- The linear substeps (4.3a) and (4.3c) only consist in solving two linear systems with the same matrix. For a fixed time step  $\tau$  such matrix is even the same at any time, which is advantageous since a preconditioner or a full Cholesky factorization can be computed just once at the beginning of the simulation.
- For the nonlinear substep it is necessary to solve the nonlinear system (4.3b); where we have canceled matrix  $M$  at both sides. The resulting nonlinear system is completely independent for each component of vector  $U_h^{(2)}$ , and as such, highly parallelizable. If we apply the Newton's method to (4.3b) each linear iteration  $s$  reads

$$\left(I + \frac{\tau}{2}D_f(U_h^{(2,s)})\right)\delta^{(s)} = b_s, \quad (4.4a)$$

$$U_h^{(2,s+1)} = U_h^{(2,s)} - \delta^{(s)}, \quad (4.4b)$$

where  $b_s = U_h^{(2,s)} - U_h^{(1)} + \frac{\tau}{2}(f(U_h^{(2,s)}) + f(U_h^{(1)}))$  and  $D_f(U_h)$  is the diagonal matrix  $D_f(U_h) = \text{diag}(f'(U_h))$ . Since matrix  $\left(I + \frac{\tau}{2}D_f(U_h^{(2,s)})\right)$  is also diagonal, the solution of (4.4a) reduces to a trivial entry-by-entry division.

- Since matrix  $\left(M + \frac{\tau}{4}A\right)$  is symmetric and positive definite, the existence of the solution of each linear substep is guaranteed. On the other hand, each independent one dimensional problem in the nonlinear substeps is equivalent to find a fixed point of function  $g(x) = a - \frac{\tau}{2}f(x)$  for some constant  $a$ , which can be trivially proven to be a contraction as long as  $0 < \tau < 2/L_f$ ; therefore, under such condition, the existence of the solution of the nonlinear substeps is also guaranteed. Existence and uniqueness of the full step in (4.2) would then proceed from those of each substep.

- The proposed scheme can be easily extended to systems of reaction-diffusion equations modeling the chemical interaction between  $p$  species as:

$$\begin{aligned} \frac{\partial}{\partial t} c_i(\mathbf{x}, t) &= \nabla \circ (\sigma_i \nabla c_i(\mathbf{x}, t)) + f_i(\mathbf{c}(\mathbf{x}, t)), & \text{in } Q_T, \text{ for } i = 1, 2, \dots, p. \\ \nabla c_i \cdot \vec{n} &= 0, & \text{on } \partial\Omega \times (0, T], \text{ for } i = 1, 2, \dots, p. \\ \mathbf{c}(\mathbf{x}, 0) &= \mathbf{c}_0(\mathbf{x}), & \text{in } \Omega. \end{aligned}$$

In such case, diffusion substeps (4.3a) and (4.3c) remain the same and are independent for each component  $c_i$ , while the reaction substep (4.3b) consists of a set of completely independent small  $p$ -dimensional nonlinear problems that can be easily solved as before.

## 5. Numerical experiments

In this section we present some numerical experiments to show the efficiency and accuracy of the proposed scheme. An object oriented implementation in MATLAB was developed for high order approximations on general polygonal meshes. As time marching scheme we use the SS-OS method (4.2) presented in section 4. All the linear systems were solved with the preconditioned conjugate gradient (PCG) method and the incomplete Cholesky factorization of MATLAB with a drop tolerance of  $10^{-5}$  was used as preconditioner. Linear and nonlinear systems were solved with a tolerance of  $10^{-8}$  as stopping criteria. Numerical quadratures for each polygon were obtained using the Vianello approach [28]. The sets of meshes used in all the experiments are exemplified in Fig. 2.

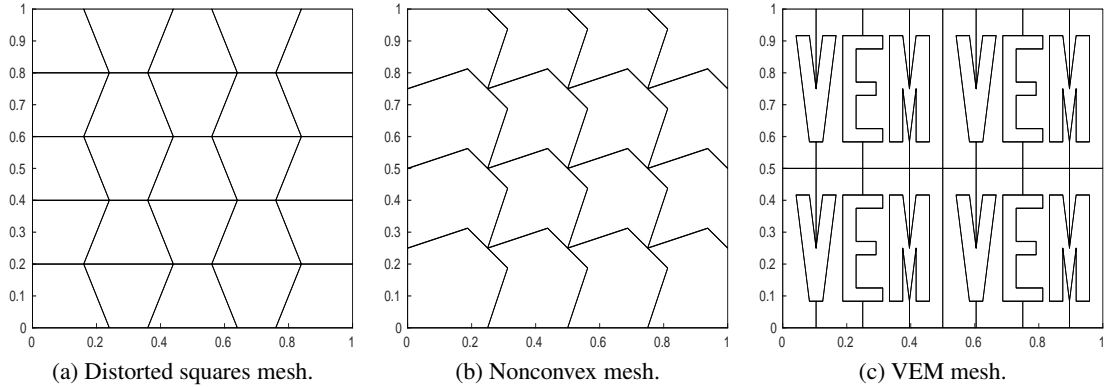


Figure 2: Example of meshes used in the numerical experiments.

In order to illustrate the efficiency of the proposed method, we will compare our results with those obtained for the non-interpolatory S-VEM, which is obtained by replacing the interpolatory term in the semi-discrete formulation (2.11a) by  $m_h(\pi_k^\partial(f(u_h)); v_h)$ . While the linear substeps of the SS-OS time marching scheme are the same for both versions, the nonlinear substeps now require to solve a system of nonlinear equations of the form

$$MU_h^{(2)} = MU_h^{(1)} - \frac{\tau}{2} \left( f_h(U_h^{(1)}) + f_h(U_h^{(2)}) \right), \quad (5.1)$$

where  $f_h(\cdot)$  is the nonlinear operator satisfying  $\langle f_h(U_h), V_h \rangle = m_h(\pi_k^\partial(f(u_h)); v_h)$ ,  $\forall v_h \in V_k^S(\mathcal{T}_h)$ .

The nonlinear systems (5.1) will be solved using a semilinear iterative method, that avoids computing the Jacobian of the nonlinear term. Each iteration  $s$  requires solving the linear system

$$MU_h^{(2,s+1)} = MU_h^{(1)} - \frac{\tau}{2} \left( f_h \left( U_h^{(1)} \right) + f_h \left( U_h^{(2,s)} \right) \right).$$

On the other hand, the reported execution times correspond to computations carried out on a DELL laptop with an Intel Core i7-8750h processor, 32Gb of RAM memory and Linux operating system.

### 5.1. Accuracy test

As first experiment we numerically asses the accuracy of the proposed method. We consider a manufactured problem on  $Q_T = (0, 1)^2 \times (0, 1]$  with a nonlinear term  $f(u) = 1/(1 + u^2)$ , adding a source term such that the exact solution be  $u(x, y, t) = e^{-t} \cos(\pi x) \cos(\pi y)$ .

In Fig. 3 we present the errors in the  $L_2$  norm of  $\pi_k^\partial(u_h)$  at the final time for each kind of meshes, with approximations up to the maximum degree allowed, i.e.,  $k = 3$  (for the distorted square meshes),  $k = 4$  (for the nonconvex meshes) and  $k = 5$  (for the VEM meshes). In the same plot we have included the errors obtained for the non-interpolatory S-VEM as reference; and no significant accuracy loss is observed for the proposed method. Optimal rates of convergence of order  $O(h^{k+1})$  are observed in each case as stated in Theorem 1. The time step was taken as  $\tau = O(h^{(k+1)/2})$  in order to equilibrate the errors in space and time.

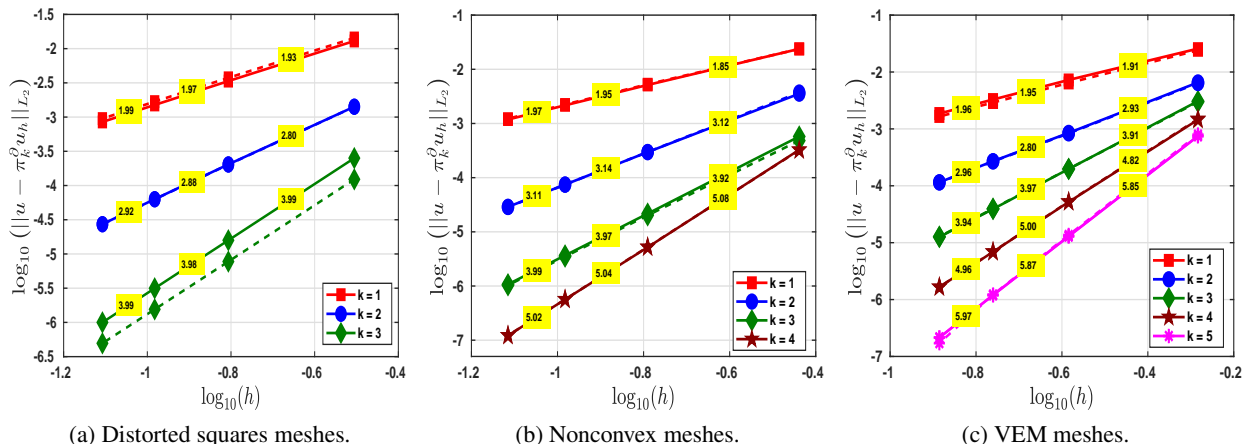


Figure 3: Rates of convergence for  $\pi_k^\partial(u_h)$  in the  $L_2$ -norm at  $T = 1$ , for the interpolatory (continuous line) and non interpolatory (dashed line) Serendipity Virtual Element methods. The numbers in the yellow rectangles are the algebraic convergence rates in  $h$  and not visible lines were overlapped.

To evaluate the temporal accuracy of the fully-discrete method, we use a sequence of time refinements with  $\tau = 1.25 \times 10^{-1}$ ,  $6.25 \times 10^{-2}$ ,  $3.125 \times 10^{-2}$ ,  $1.5625 \times 10^{-2}$ ; and in order to let the time error dominate, computations were carried out for the finest mesh of each kind and the maximum degree allowed. The obtained rates of convergence for the  $\mathcal{DRD}$  and the  $\mathcal{RDR}$  splitting methods are depicted in Fig. 4 and validate the second order  $O(\tau^2)$  accuracy of the OS-SS time marching scheme. In this experiment, better accuracy is observed for the  $\mathcal{RDR}$  splitting for all the meshes.

In Table 1 we present the number of global degrees of freedom for the Serendipity VEM and the classical VEM, where naturally a more significant reduction is obtained at increasing  $k$ .

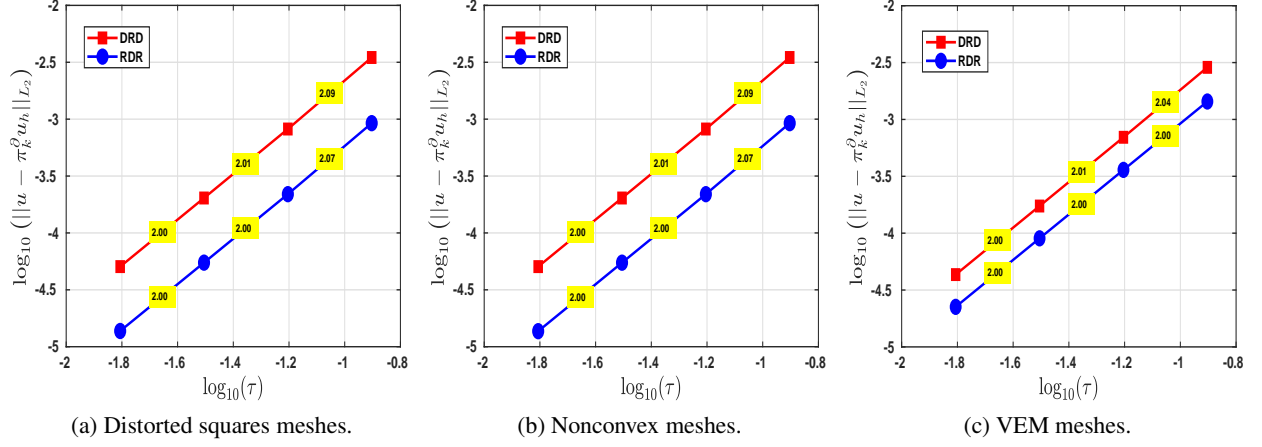


Figure 4: Time accuracy of the proposed method at  $T = 1$  for both versions of the fully discrete scheme (4.2).

Mesh type	VEM		Nonconvex		Distorted squares	
	S-VEM	VEM	S-VEM	VEM	S-VEM	VEM
$k = 2$						
$m_1$	<b>353</b>	381	<b>113</b>	129	<b>96</b>	121
$m_2$	<b>1369</b>	1481	<b>568</b>	649	<b>341</b>	441
$m_3$	<b>3301</b>	3409	<b>1373</b>	1569	<b>736</b>	961
$m_4$	<b>5393</b>	5841	<b>2528</b>	2889	<b>1281</b>	1681
$k = 3$						
$m_1$	<b>543</b>	627	<b>177</b>	225	<b>156</b>	231
$m_2$	<b>2109</b>	2445	<b>892</b>	1135	<b>561</b>	861
$m_3$	<b>4699</b>	5455	<b>1135</b>	2157	<b>1216</b>	1891
$m_4$	<b>8313</b>	9657	<b>3972</b>	5055	<b>2121</b>	3321
$k = 4$						
$m_1$	<b>733</b>	901	<b>241</b>	337	—	—
$m_2$	<b>2849</b>	3521	<b>1216</b>	1702	—	—
$m_3$	<b>6349</b>	7861	<b>2941</b>	4117	—	—
$m_4$	<b>11233</b>	13921	<b>5416</b>	7582	—	—
$k = 5$						
$m_1$	<b>923</b>	1203	—	—	—	—
$m_2$	<b>3589</b>	4709	—	—	—	—
$m_3$	<b>7999</b>	10519	—	—	—	—
$m_4$	<b>14153</b>	18633	—	—	—	—

Table 1: Comparison in terms of the number of degrees of freedom for the S-VEM and the classical VEM.

## 5.2. Efficiency tests

### 5.2.1. Allen-Cahn simulation

In this experiment we consider the following Allen-Cahn equation on  $Q_T = (0, 1)^2 \times (0, T]$  as in [1]:

$$\frac{\partial u}{\partial t} - \epsilon \Delta u + u^3 - u = 0, \quad \text{in } Q_T, \quad (5.2a)$$

$$\nabla u \cdot \vec{n} = 0, \quad \text{on } \partial\Omega \times (0, T), \quad (5.2b)$$

$$u(\mathbf{x}, 0) = \cos(2\pi x^2) \cos(2\pi y^2), \quad \text{on } \Omega, \quad (5.2c)$$

where the nonlinear term  $f(u) = u^3 - u$  only satisfies a local Lipschitz condition.

In Figures 5-6 we show the evolution of the approximated solutions  $\pi_k^\partial(u_h)$  for the Allen-Cahn equation with  $\epsilon = 0.1$  and  $\epsilon = 0.01$ , respectively; which are expected to converge to their corresponding stable states  $u = 1$ , and  $u = -1$ . The computations were carried out for the  $\mathcal{RDR}$  splitting scheme with time step  $\tau = 5 \times 10^{-2}$ ; and spatial approximations with  $k = 4$  on a non-convex mesh of size  $h \approx 7.67 \times 10^{-2}$ . The plots portray the same behaviour presented by Adak *et. al.*, in [1] for the classical VEM with non-interpolatory treatment of the nonlinear term.

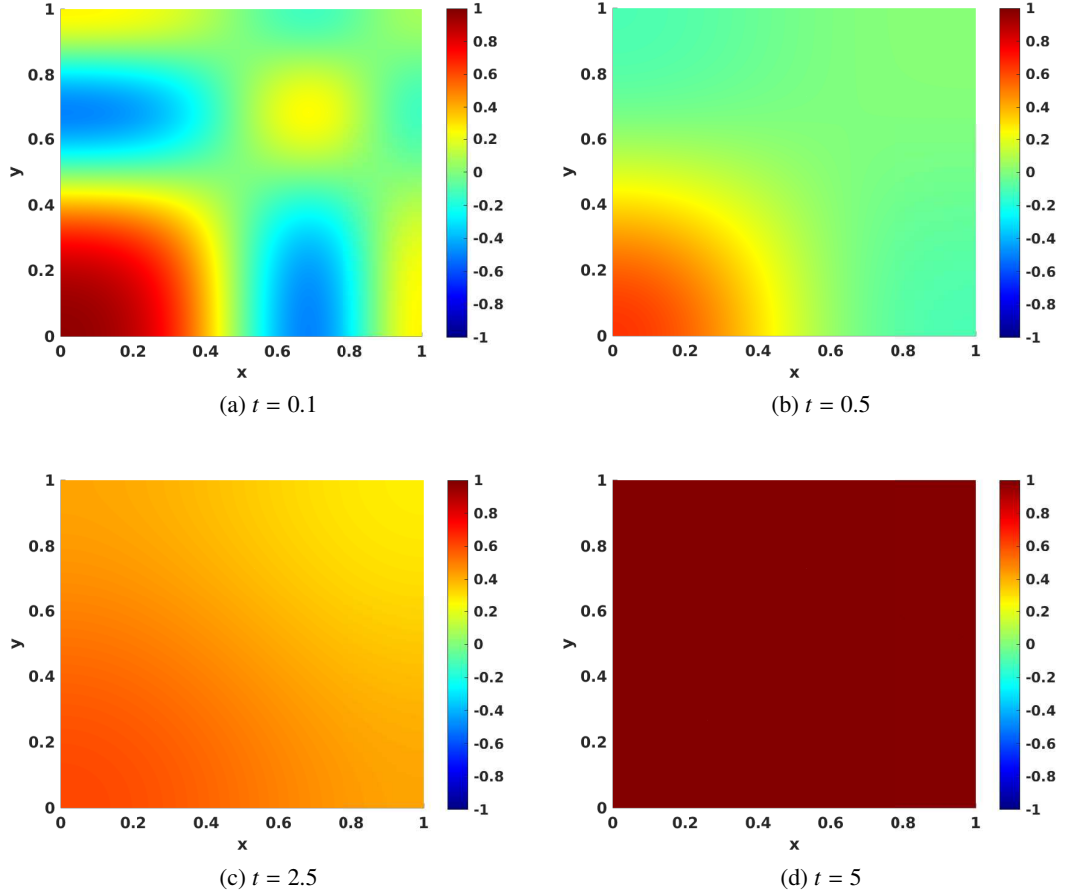


Figure 5: Snapshots of the approximation  $\pi_k^\partial(u_h)$  for the Allen-Cahn equation (5.2) with  $\epsilon = 0.1$ .

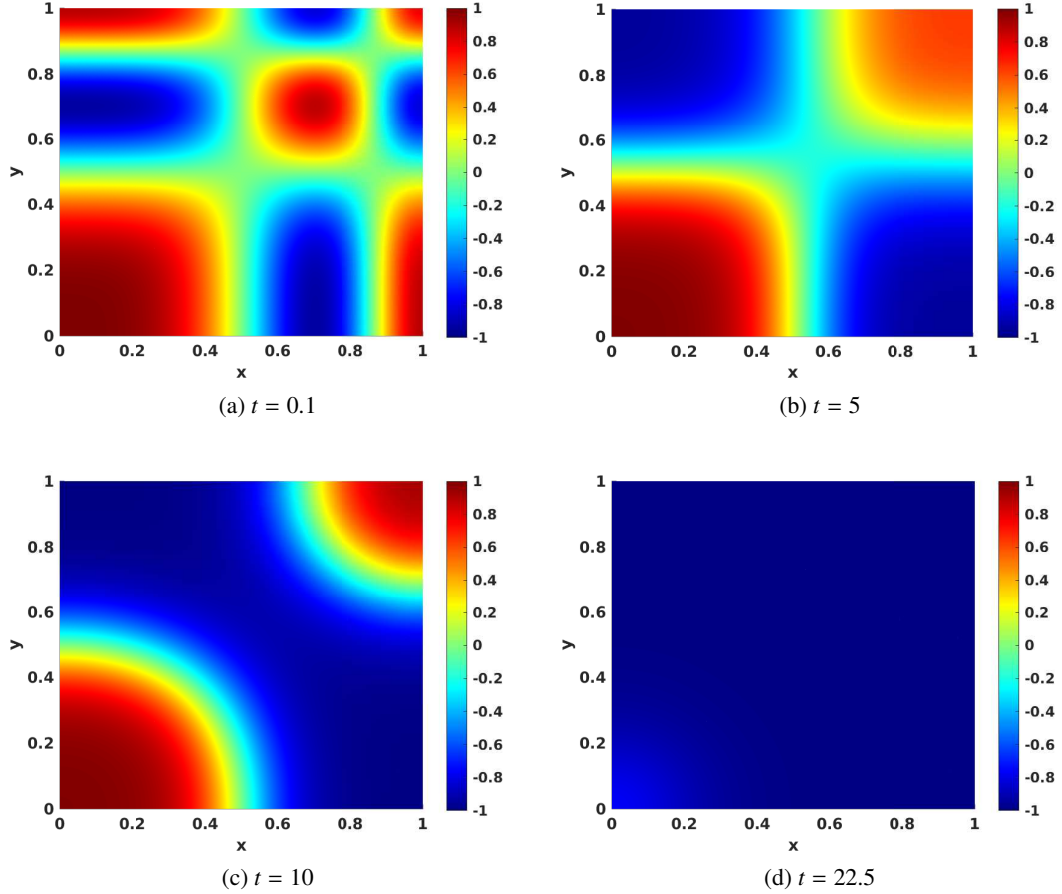


Figure 6: Snapshots of the approximation  $\pi_k^\partial(u_h)$  for the Allen-Cahn equation (5.2) with  $\epsilon = 0.01$ .

In order to show the efficiency of the proposed method, in Table 2 we report the CPU execution times for the interpolatory and non-interpolatory Serendipity Virtual Element methods. We observe that the time for the linear substeps are approximately equal in both cases, as expected. However, for the nonlinear substeps our method performs about 200 times faster than the non-interpolatory S-VEM. As a result, we obtain a total boost of approximately 8 times with respect to the classical S-VEM. We must point out, that if a full Newton's iteration were to be used to solve the nonlinear system (5.1), the computational cost of the non-interpolatory version would dramatically increase, due to the expensive evaluation of the Jacobian of the nonlinear term. In a similar way, the classical VEM formulation presented in [1] is expected to have an even higher computational cost, due to the increase in the number of degrees of freedom.

Linear substeps			Nonlinear substeps			Total		
iS-VEM (sec)	S-VEM (sec)	Ratio	iS-VEM (sec)	S-VEM (sec)	Ratio	iS-VEM (sec)	S-VEM (sec)	Ratio
91.12	101.08	<b>1.11</b>	7.88	1596.87	<b>202.65</b>	99	1697.95	<b>8.37</b>

Table 2: CPU execution times for the Allen-Cahn equation (5.2) with  $\epsilon = 0.01$ , for the interpolatory (iS-VEM) and non-interpolatory (S-VEM) Serendipity Virtual Element methods.

### 5.2.2. Schnakenberg system [27]

The Schnakenberg model is a system of reaction-diffusion equations that models the spatial distribution of a morphogen and it is commonly used as benchmark for numerical methods applied to this kind of problems. The model is usually formulated on  $Q = (0, 1)^2 \times (0, T]$  as follows:

$$\frac{\partial c_a}{\partial t} = D_1 \Delta c_a + \kappa (a - c_a + c_a^2 c_i), \quad \text{in } \Omega \times (0, T], \quad (5.3a)$$

$$\frac{\partial c_i}{\partial t} = D_2 \Delta c_i + \kappa (b - c_a^2 c_i), \quad \text{in } \Omega \times (0, T], \quad (5.3b)$$

where  $c_a$  and  $c_i$  are the concentrations of the activator and the inhibitor, respectively. We take as initial conditions:

$$c_a^0(x, y) = a + b + 10^{-3} e^{-100((x-1/3)^2 + (y-1/2)^2)}, \quad \text{and} \quad c_i^0(x, y) = \frac{b}{(a+b)^2},$$

and the parameters choice:  $\kappa = 100$ ,  $a = 0.1305$ ,  $b = 0.7695$ ,  $D_1 = 0.05$  and  $D_2 = 1$ .

In Figure 7 we plot the numerical approximation  $\pi_k^\partial(c_{a,h})$  of the activator, for  $k = 3$  and a distorted squares mesh of size  $h \approx 3.12 \times 10^{-2}$ . In this simulation we used the  $\mathcal{RDR}$  splitting time discretization with  $\tau = 1 \times 10^{-3}$ ; and the expected spot pattern is exhibited. The execution times for this experiment are reported in Table 3, where a total performance boost of around 10 times is obtained for the interpolatory S-VEM.

Diffusion substeps			Reaction substeps			Total		
iS-VEM (sec)	S-VEM (sec)	Ratio	iS-VEM (sec)	S-VEM (sec)	Ratio	iS-VEM (sec)	S-VEM (sec)	Ratio
161.71	168.95	<b>1.04</b>	477.60	6504.97	<b>13.62</b>	639.31	6673.92	<b>10.44</b>

Table 3: CPU execution times for the interpolatory (iS-VEM) and non-interpolatory (S-VEM) Serendipity Virtual Element methods for the Schnakenberg system (5.3).

## 6. Conclusions

In this work an interpolatory Serendipity Virtual Element method for semilinear parabolic problems on polygonal meshes is proposed. A significant reduction in the computational cost of the method is obtained by approximating the nonlinear term with its interpolant in the S-VEM space; while the number of degrees of freedom is smaller compared with traditional VEM. Optimal error estimates of order  $O(h^{k+1})$  in the  $L_2$ -norm are proven for the semi-discrete formulation.

To exploit the structure of the resulting system of nonlinear differential equations from the semi-discrete formulation, we combine it with a second order operator splitting technique, which decouples the linear and nonlinear terms. In turn, nonlinear substeps are readily decomposed as a set of small completely independent one dimensional nonlinear equations. Our numerical experiments validate the optimal convergence of the method and the improvement in efficiency is clearly evidenced. The extension of the idea in this work to three dimensional problems and a proper comparison of different time discretizations is an ongoing work.

## References

[1] D. Adak, E. Natarajan, and S. Kumar. Convergence analysis of virtual element methods for semilinear parabolic problems on polygonal meshes. *Num. Meth. for PDEs*, 35(1):222–245, 2019.

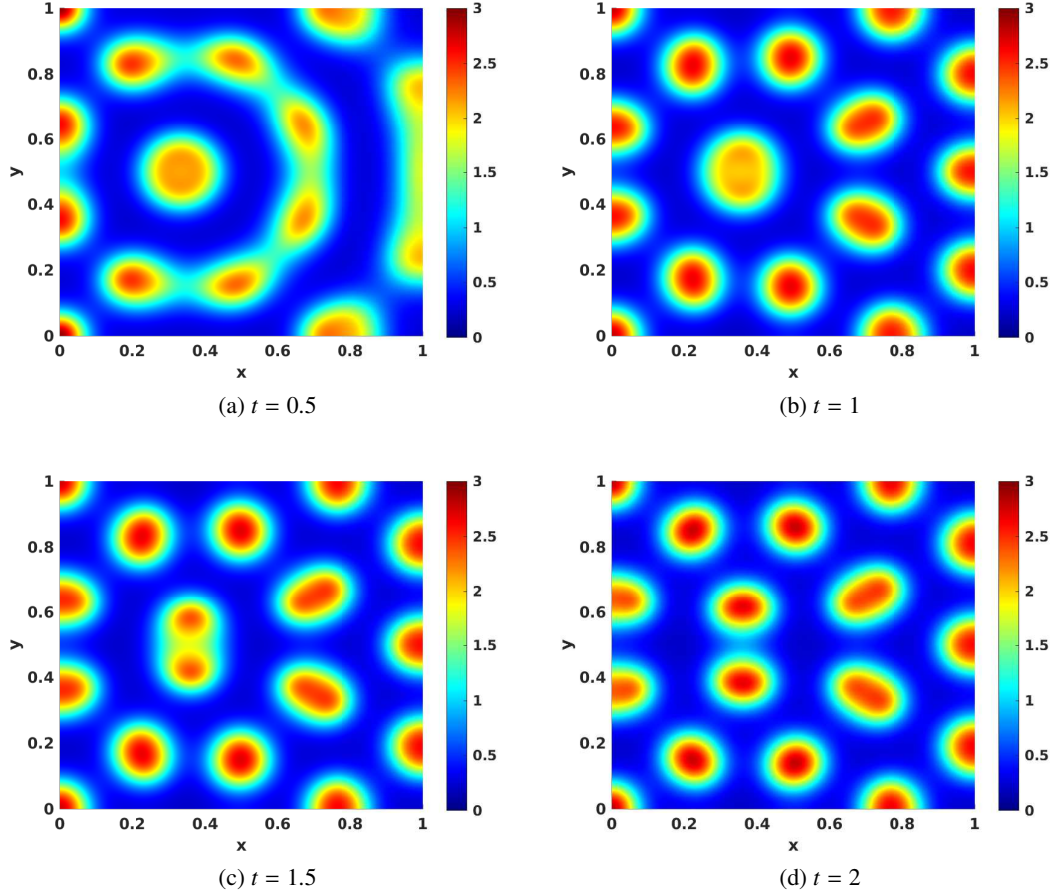


Figure 7: Snapshots of the approximation  $\pi_k^\partial(c_{a,h})$  for the Schnakenberg system (5.3).

- [2] D. Adak, E. Natarajan, and S. Kumar. Virtual element method for semilinear hyperbolic problems on polygonal meshes. *Int. J. of Comp. Math.*, 96(5):971–991, 2019.
- [3] D. Adak and S. Natarajan. Virtual element method for semilinear sine–Gordon equation over polygonal mesh using product approximation technique. *Math. & Comp. in Simul.*, 172:224–243, 2020.
- [4] D. Adak and S. Natarajan. Virtual element methods for nonlocal parabolic problems on general type of meshes. *Adv. in Comp. Math.*, 46(5):1–29, 2020.
- [5] D. Adak, S. Natarajan, and E. Natarajan. Virtual element method for semilinear elliptic problems on polygonal meshes. *Appl. Num. Math.*, 145:175–187, 2019.
- [6] B. Ahmad, A. Alsaedi, F. Brezzi, D. Marini, and A. Russo. Equivalent projectors for virtual element methods. *Computers & Mathematics with Applications*, 66(3):376–391, 2013.
- [7] V. Anaya, M. Bendahmane, D. Mora, and M. Sepúlveda. A virtual element method for a nonlocal Fitzhugh–Nagumo model of cardiac electrophysiology. *IMA J. of Num. Anal.*, 40(2):1544–1576, 2020.
- [8] P. Antonietti, L. da Veiga, S. Scacchi, and M. Verani. A  $C^1$  virtual element method for the Cahn–Hilliard equation with polygonal meshes. *SIAM J. Num. Anal.*, 54(1):34–56, 2016.
- [9] S. Brenner and L. Scott. *The mathematical theory of finite element methods*, volume 3. Springer, 2008.
- [10] A. Cangiani, P. Chatzipantelidis, G. Diwan, and E. Georgoulis. Virtual element method for quasilinear elliptic problems. *IMA J. Num. Anal.*, 40(4):2450–2472, 2020.
- [11] G. Cantor. A contribution to the theory of diversity. *Journal for Pure and Applied Mathematics (Crelles Journal)*, 1878(84):242–258, 1878.
- [12] P. Castillo and S. Gómez. Interpolatory super-convergent discontinuous Galerkin methods for nonlinear reaction diffusion

equations on three dimensional domains. *Commun. in Nonl. Sci. and Num. Simul.*, 90(C):105388, 2020.

[13] P. Castillo and S. Gómez. An interpolatory directional splitting-local discontinuous Galerkin method with application to pattern formation in 2D/3D. *Appl. Math. and Comp.*, 397(C):125984, 2021.

[14] L. da Veiga, F. Brezzi, A. Cangiani, G. Manzini, L. Marini, and A. Russo. Basic principles of virtual element methods. *Math. Models Methods Appl. Sci.*, 23(01):199–214, 2013.

[15] L. da Veiga, F. Brezzi, L. Marini, and A. Russo. The hitchhiker’s guide to the virtual element method. *Math. Models Methods Appl. Sci.*, 24(08):1541–1573, 2014.

[16] L. da Veiga, F. Brezzi, L. Marini, and A. Russo. Serendipity nodal VEM spaces. *Computers & Fluids*, 141:2–12, 2016.

[17] L. da Veiga, C. Lovadina, and A. Russo. Stability analysis for the virtual element method. *Math. Models and Methods in Appl. Sci.*, 27(13):2557–2594, 2017.

[18] M. Davis. *Computability and Unsolvability*. McGraw-Hill, New York, 1958.

[19] M. Frittelli, A. Madzvamuse, and I. Sgura. Bulk-surface virtual element method for systems of PDEs in two-space dimensions. *Numer. Math.*, 147(2):305–348, 2021.

[20] R. Kobayashi. Modeling and numerical simulations of dendritic crystal growth. *Phys. D: Nonlinear Phenomena*, 63(3-4):410–423, 1993.

[21] X. Liu, Z. He, and Z. Chen. A fully discrete virtual element scheme for the Cahn–Hilliard equation in mixed form. *Comp. Phys. Commun.*, 246:106870, 2020.

[22] L. Marcon and J. Sharpe. Turing patterns in development: what about the horse part? *Current opinion in genetics & development*, 22(6):578–584, 2012.

[23] L. Mascotto. Ill-conditioning in the virtual element method: Stabilizations and bases. *Num. Meth. Part. Diff. Eqs.*, 34(4):1258–1281, 2018.

[24] A. Mikhailov and K. Showalter. Control of waves, patterns and turbulence in chemical systems. *Phys. Reports*, 425(2-3):79–194, 2006.

[25] M. Neubert and H. Caswell. Demography and dispersal: calculation and sensitivity analysis of invasion speed for structured populations. *Ecology*, 81(6):1613–1628, 2000.

[26] A. Russo. On the choice of the internal degrees of freedom for the nodal virtual element method in two dimensions. *Comp. & Math. with Appl.*, 72(8):1968–1976, 2016.

[27] J. Schnakenberg. Simple chemical reaction systems with limit cycle behaviour. *J. of theoretical biology*, 81(3):389–400, 1979.

[28] A. Sommariva and M. Vianello. Product Gauss cubature over polygons based on Green’s integration formula. *BIT Num. Math.*, 47(2):441–453, 2007.

[29] G. Strang. On the construction and comparison of difference schemes. *SIAM J. Num. Anal.*, 5(3):506–517, 1968.

[30] A. Tenno, R. Tenno, and T. Suntio. Charge–discharge behaviour of VRLA batteries: model calibration and application for state estimation and failure detection. *J. of Power Sources*, 103(1):42–53, 2001.

[31] A. Turing. The chemical basis of morphogenesis. *Bulletin of Mathematical Biology*, 52(1):153–197, 1990.

[32] G. Vacca and L. da Veiga. Virtual element methods for parabolic problems on polygonal meshes. *Num. Meth. Part. Diff. Eqs.*, 31(6):2110–2134, 2015.

## Appendix A Implementation details

For the sake of completeness we dedicate this appendix to provide a guide on the computations of the matrices required in the implementation of the proposed method. Even though the ideas here are similar to those presented in [15, 16], the main difference in the serendipity VEM is the appearance of projector  $\pi_k^0(\cdot)$  which becomes the seed for computing all the matrices. More specifically, we need to take into account that the computation of  $\pi_{k,E}^V(v)$  makes use of all the moments of  $v$  up to degree  $k$ , which in turn coincide with those of  $\pi_k^0(v)$  by definition of  $V_k^S(\mathcal{T}_h)$ .

It will be useful when integrating over an edge, to denote by  $\{\omega_i^{\text{Leg}}, z_i^{\text{Leg}}\}_{i=1}^{k+1}$  and  $\{\omega_i^{\text{Lob}}, z_i^{\text{Lob}}\}_{i=1}^{k+1}$  the Gauss-Legendre and Gauss-Lobatto quadrature pairs on  $[-1, 1]$ ; and by  $\{L_i^{\text{Lob}}(t)\}_{i=1}^{k+1}$  the Lagrange polynomials of degree  $k$  associated to the Gauss-Lobatto points.

The computation of the local contributions to each global matrix is done as follows. First of all it is necessary to provide a basis (from the many possibilities) for the space  $\mathbb{P}_k(E)$ ; for simplicity, we choose the following scaled monomial basis which has been widely used in VEM implementations:

$$\mathcal{M}_k(E) := \left\{ m_{\alpha} \in \mathbb{P}_k(E) \mid m_{\alpha}(x, y) = \left( \frac{x - x_b}{h_E} \right)^{\alpha_x} \left( \frac{y - y_b}{h_E} \right)^{\alpha_y}, \quad 0 \leq |\alpha| \leq k \right\}, \quad (\text{A.1})$$

where  $|\alpha| = \alpha_x + \alpha_y$ ,  $h_E = \text{diam}(E)$ , and  $(x_b, y_b) \in \mathbb{R}^2$  is the barycenter of  $E$ . The number of scaled monomials in  $\mathcal{M}_k(E)$  is denoted by  $r_k = \dim(\mathbb{P}_k(E)) = \frac{(k+1)(k+2)}{2}$ .

To simplify the notation we need to sort the elements of  $\mathcal{M}_k(E)$ ; an explicit practical way, and also useful in the code, is to use the Cantor's pairing function [11], which is a map  $\rho : \mathbb{N}^2 \rightarrow \mathbb{N}$  defined by

$$\rho(\alpha) := \frac{|\alpha|(|\alpha| + 1)}{2} + \alpha_y + 1, \quad \forall \alpha = (\alpha_x, \alpha_y) \in \mathbb{N}^2;$$

that in addition is bijective and its inverse can also be obtained explicitly [18]. Since  $\rho(\cdot)$  uniquely identifies each multi-index  $\alpha$  such that  $0 \leq |\alpha| \leq k$ , with a number  $\rho(\alpha) \in \{1, \dots, r_k\}$ , we can incur in a slight abuse of notation using indistinctly  $\alpha$  and  $\alpha = \rho(\alpha)$ .

### A.1 Construction of auxiliary matrices

By definition, for each basis function  $\phi_i \in V_k^S(E)$ ;  $\pi_k^{\partial}(\phi_i)$  and  $\pi_k^{\nabla}(\phi_i)$  belong to  $\mathbb{P}_k(E)$  and as such, they must have a representation in the basis  $\mathcal{M}_k(E)$  of the form

$$\pi_k^{\partial}(\phi_i) = \sum_{\alpha=1}^{r_k} s_{\alpha,i}^{\partial} m_{\alpha}, \quad \pi_k^{\nabla}(\phi_i) = \sum_{\alpha=1}^{r_k} s_{\alpha,i}^{\nabla} m_{\alpha}. \quad (\text{A.2})$$

As becomes clear later, it is convenient to arrange these representation coefficients in two matrices  $S^{\partial}$  and  $S^{\nabla}$  of size  $r_k \times d_k^S$  as:

$$S^{\partial} = \begin{pmatrix} s_{1,1}^{\partial} & s_{1,2}^{\partial} & \dots & s_{1,d_k^S}^{\partial} \\ s_{2,1}^{\partial} & s_{2,2}^{\partial} & \dots & s_{2,d_k^S}^{\partial} \\ \vdots & \vdots & & \vdots \\ s_{r_k,1}^{\partial} & s_{r_k,2}^{\partial} & \dots & s_{r_k,d_k^S}^{\partial} \end{pmatrix}, \quad S^{\nabla} = \begin{pmatrix} s_{1,1}^{\nabla} & s_{1,2}^{\nabla} & \dots & s_{1,d_k^S}^{\nabla} \\ s_{2,1}^{\nabla} & s_{2,2}^{\nabla} & \dots & s_{2,d_k^S}^{\nabla} \\ \vdots & \vdots & & \vdots \\ s_{r_k,1}^{\nabla} & s_{r_k,2}^{\nabla} & \dots & s_{r_k,d_k^S}^{\nabla} \end{pmatrix}$$

which by the definition of their corresponding projections must satisfy the following linear matrix equations:

- From (2.4) matrix  $S^{\partial}$  must satisfy  $BS^{\partial} = R^{\partial}$ , for matrices  $B \in \mathbb{R}^{r_k \times r_k}$  and  $R^{\partial} \in \mathbb{R}^{r_k \times d_k^S}$  given by

$$B = \begin{pmatrix} (m_1; m_1)_{\partial E} & (m_1; m_2)_{\partial E} & \dots & (m_1; m_{r_k})_{\partial E} \\ (m_2; m_1)_{\partial E} & (m_2; m_2)_{\partial E} & \dots & (m_2; m_{r_k})_{\partial E} \\ \vdots & \vdots & \ddots & \vdots \\ (m_{r_k}; m_1)_{\partial E} & (m_{r_k}; m_2)_{\partial E} & \dots & (m_{r_k}; m_{r_k})_{\partial E} \end{pmatrix}, \quad R^{\partial} = \begin{pmatrix} (m_1; \phi_1)_{\partial E} & (m_1; \phi_2)_{\partial E} & \dots & (m_1; \phi_{d_k^S})_{\partial E} \\ (m_2; \phi_1)_{\partial E} & (m_2; \phi_2)_{\partial E} & \dots & (m_2; \phi_{d_k^S})_{\partial E} \\ \vdots & \vdots & \ddots & \vdots \\ (m_{r_k}; \phi_1)_{\partial E} & (m_{r_k}; \phi_2)_{\partial E} & \dots & (m_{r_k}; \phi_{d_k^S})_{\partial E} \end{pmatrix},$$

where we must point out that matrix  $B$  only involves line integrals of polynomials on the edges of  $E$  and under our restriction  $k < \eta_E$  it is nonsingular.

For each edge  $e \subset \partial E$ , if we denote by  $\{\ell_i^e\}_{i=1}^{k+1}$  the indices of those degrees of freedom “living“ on  $e$ , the restriction of a function  $v_h \in V_k^S(E)$  to  $e$  can be parametrically written as a one dimensional

polynomial of degree  $k$ , i.e., for some linear map  $\vartheta_e : [-1, 1] \rightarrow e$

$$v_h|_e(\vartheta_e(t)) = \sum_{i=1}^{k+1} \text{dof}_{\ell_i^e}(v_h) L_i^{\text{Lob}}(t), \quad \forall t \in [-1, 1],$$

then for all  $m_{\alpha} \in \mathcal{M}_k(E)$ , using the degrees of freedom of  $v_h$  and the Gauss-Legendre quadrature rule, which is exact polynomials up to degree  $2k + 1$ , we can compute

$$\int_e m_{\alpha} v_h dS = \frac{|e|}{2} \sum_{l=1}^{k+1} \omega_l^{\text{Leg}} \left( \sum_{i=1}^{k+1} \text{dof}_{\ell_i^e}(v_h) L_i^{\text{Lob}}(z_l^{\text{Leg}}) \right) m_{\alpha}(\vartheta_e(z_l^{\text{Lob}})),$$

where  $|e|$  is the length of edge  $e$ .

In particular, the assembling of matrix  $R^{\partial}$  reduces to compute, on each edge  $e$  of  $E$ , and for each VEM basis function  $\phi_{\ell_j^e}$  and  $m_{\alpha} \in \mathcal{M}_k(E)$

$$\int_e m_{\alpha} \phi_{\ell_j^e} dS \stackrel{(2.7)}{=} \frac{|e|}{2} \sum_{l=1}^{k+1} \omega_l^{\text{Leg}} L_j^{\text{Lob}}(z_l^{\text{Leg}}) m_{\alpha}(\vartheta_e(z_l^{\text{Lob}})). \quad (\text{A.3})$$

- From (2.2), matrix  $S^{\nabla}$  satisfies  $GS^{\nabla} = R^{\nabla}$ , where

$$G = \begin{pmatrix} \pi_o(m_1) & \pi_o(m_2) & \dots & \pi_o(m_{r_k}) \\ 0 & a^E(m_2; m_2) & \dots & a^E(m_2; m_{r_k}) \\ \vdots & \vdots & \ddots & \vdots \\ 0 & a^E(m_{r_k}; m_2) & \dots & a^E(m_{r_k}; m_{r_k}) \end{pmatrix}, \quad R^{\nabla} = \begin{pmatrix} \pi_o(\phi_1) & \dots & \pi_o(\phi_{d_k^S}) \\ a^E(m_2; \phi_1) & \dots & a^E(m_2; \phi_{d_k^S}) \\ \vdots & \vdots & \vdots \\ a^E(m_{r_k}; \phi_1) & \dots & a^E(m_{r_k}; \phi_{d_k^S}) \end{pmatrix},$$

and as before matrix  $G$  is nonsingular and only involves volume integrals on  $E$  of polynomial products.

Regarding the entries of matrix  $R^{\nabla}$ ; for  $k = 1$  the first row can be computed as in Eqn. (A.3) for  $m_1 \equiv 1$ ; while for  $k > 1$ , the entries are given by

$$\int_E \phi_j d\mathbf{x} \stackrel{(2.5)}{=} \int_E \pi_k^{\partial}(\phi_j) d\mathbf{x} \stackrel{(\text{A.2})}{=} \sum_{\alpha=1}^{r_k} s_{\alpha,j}^{\partial} \int_E m_{\alpha} d\mathbf{x},$$

so the first row of  $R^{\nabla}$  can be obtained as  $L^T S^{\partial}$  where  $L \in \mathbb{R}^{r_k}$  is a column vector with entries:  $\int_E m_{\alpha} d\mathbf{x}$ .

For the remaining rows of  $R^{\nabla}$ , by Green's identity, we need to compute

$$\int_E \nabla \phi_j \cdot \nabla m_{\alpha} d\mathbf{x} = \int_{\partial E} \phi_j \nabla m_{\alpha} \cdot \vec{n} dS - \int_E \phi_j \Delta m_{\alpha} d\mathbf{x}, \quad (\text{A.4})$$

where the argument in the first term at the right-hand side of (A.4) restricted to each edge  $e$  is a polynomial of degree  $2k - 1$ , and can be easily computed similar as in (A.3) but using instead the Gauss-Lobatto rule as

$$\int_e \phi_{\ell_j^e} \nabla m_{\alpha} \cdot \vec{n} dS = \frac{|e|}{2} \omega_j^{\text{Lob}} \nabla m_{\alpha}(\vartheta_e(z_j^{\text{Lob}})) \cdot \vec{n},$$

this is in fact the same as for the classical VEM. The most significant change concerns to the second term at the right-hand side of (A.4). If we represent  $\Delta m_{\alpha} \in \mathbb{P}_k(E)$  in the basis  $\mathcal{M}_{k-2}(E)$  as

$$\Delta m_{\alpha} = \sum_{\beta=1}^{r_{k-2}} \zeta_{\alpha,\beta} m_{\beta}, \quad (\text{A.5})$$

the entries of the second term can then be computed as

$$\int_E \phi_j \Delta m_{\alpha} dx \stackrel{(\text{A.5})}{=} \sum_{\beta=1}^{r_{k-2}} \zeta_{\alpha,\beta} \int_E \phi_j m_{\beta} dx \stackrel{(\text{2.5})}{=} \sum_{\beta=1}^{r_{k-2}} \zeta_{\alpha,\beta} \int_E \pi_k^{\partial}(\phi_j) m_{\beta} dx \stackrel{(\text{A.2})}{=} \sum_{\beta=1}^{r_{k-2}} \sum_{\gamma=1}^{r_k} \zeta_{\alpha,\beta} s_{\gamma,j}^{\partial} \int_E m_{\gamma} m_{\beta} dx,$$

so the total contribution of the second term at the right-hand side of (A.4) is given by the matrix product  $ZH^{(k-2,2)}S^{\partial}$ , where  $Z \in \mathbb{R}^{r_k \times r_{k-2}}$  and  $H^{(k-2,k)} \in \mathbb{R}^{r_{k-2} \times r_k}$  have the following structure

$$Z = \begin{pmatrix} \zeta_{1,1} & \dots & \zeta_{1,r_{k-2}} \\ \vdots & & \vdots \\ \zeta_{r_k,1} & \dots & \zeta_{r_k,r_{k-2}} \end{pmatrix}, \quad H^{(k-2,k)} = \begin{pmatrix} (m_1; m_1)_E & \dots & (m_1; m_{r_k})_E \\ \vdots & & \vdots \\ (m_{r_{k-2}}; m_1)_E & \dots & (m_{r_{k-2}}; m_{r_k})_E \end{pmatrix}. \quad (\text{A.6})$$

Indeed, matrix  $Z$  has a very simple structure due to the practical shape of the monomials in  $\mathcal{M}_k(E)$ . If we take  $\varrho_x(\alpha) = \rho^{-1}(\alpha_x - 2, \alpha_y)$  when  $\alpha_x \geq 2$  and  $\varrho_y(\alpha) = \rho^{-1}(\alpha_x, \alpha_y - 2)$  when  $\alpha_y \geq 2$ ,

$$Z_{\alpha,\beta} = \begin{cases} \frac{\alpha_x(\alpha_x - 1)}{h_E^2}, & \text{if } \beta = \varrho_x(\alpha), \alpha_x \geq 2, \\ \frac{\alpha_y(\alpha_y - 1)}{h_E^2}, & \text{if } \beta = \varrho_y(\alpha), \alpha_y \geq 2, \\ 0, & \text{otherwise.} \end{cases}$$

Finally, since  $\mathbb{P}_k(E) \subset V_k^S(E)$ , for a generic projection  $\pi_k : V_k^S(E) \rightarrow \mathbb{P}_k(E)$ , we can get a representation of  $\pi_k(\phi_i)$  in the basis of  $V_k^S(E)$  as

$$\pi_k(\phi_i) = \sum_{\alpha=1}^{r_k} s_{\alpha,i} m_{\alpha} = \sum_{\alpha=1}^{r_k} s_{\alpha,i} \sum_{j=1}^{d_k^S} \text{dof}_j(m_{\alpha}) \phi_j; \quad (\text{A.7})$$

therefore, if we denote by  $S$  the coefficients matrix associated to  $\pi_k$ , the matrix representation of  $\pi_k(\cdot)$  as an operator from  $V_k^S(E) \rightarrow V_k^S(E)$  is  $S_{\blacksquare} = DS$ , where matrix  $D \in \mathbb{R}^{d_k^S \times r_k}$  is simply

$$D = \begin{pmatrix} m_1(\xi_1) & m_2(\xi_1) & \dots & m_{r_k}(\xi_1) \\ m_1(\xi_2) & m_2(\xi_2) & \dots & m_{r_k}(\xi_2) \\ \vdots & \vdots & & \vdots \\ m_1(\xi_{d_k^S}) & m_2(\xi_{d_k^S}) & \dots & m_{r_k}(\xi_{d_k^S}) \end{pmatrix}. \quad (\text{A.8})$$

## A.2 Assembling of local matrices

As in the classical FEM, to get the contributions to each matrix in (4.1) it is only necessary to compute the values of the local bilinear forms at all the possible pair combinations of the basis functions  $\{\phi_i\}_{i=1}^{d_{k,E}^S}$ ; which after having computed the matrices of the previous section are nearly at hand as shown below.

- **Consistency stiffness matrix  $K_C^E$ :**

Noticing that

$$\begin{aligned} a^E(\pi_k^\nabla(\phi_i); \pi_k^\nabla(\phi_j)) &= \int_E \nabla(\pi_k^\nabla(\phi_i)) \cdot \nabla(\pi_k^\nabla(\phi_j)) dx = \sum_{\alpha=1}^{r_k} \sum_{\beta=1}^{r_k} s_{\alpha,i}^\nabla s_{\beta,j}^\nabla \int_E \nabla m_\alpha \cdot \nabla m_\beta dx \\ &= \sum_{\alpha=1}^{r_k} \sum_{\beta=1}^{r_k} s_{\alpha,i}^\nabla s_{\beta,j}^\nabla a^E(m_\alpha; m_\beta), \end{aligned}$$

then the contribution of the consistency term for the stiffness matrix is just

$$K_C^E = (S^\nabla)^T \tilde{G} S^\nabla \quad (\text{A.9})$$

where matrix  $\tilde{G} \in \mathbb{R}^{r_k \times r_k}$  coincides with  $G$  except by its first row, that is full of zeros, i.e.,

$$\tilde{G} = \begin{pmatrix} 0 & 0 & \dots & 0 \\ 0 & a^E(m_2; m_2) & \dots & a^E(m_2; m_{r_k}) \\ \vdots & \vdots & \ddots & \vdots \\ 0 & a^E(m_{r_k}; m_2) & \dots & a^E(m_{r_k}; m_{r_k}) \end{pmatrix}.$$

- **Stability stiffness matrix  $K_S^E$ :**

The stability term is taken as the simple choice:

$$s_a^E((I - \pi_k^\nabla)\phi_i; (I - \pi_k^\nabla)\phi_j) = \sum_{\ell=1}^{d_k^S} \text{dof}_\ell((I - \pi_k^\nabla)\phi_i) \text{dof}_\ell((I - \pi_k^\nabla)\phi_j),$$

therefore

$$K_S^E = (I_{d_k^S} - S_\bullet^\nabla)^T (I_{d_k^S} - S_\bullet^\nabla) \quad (\text{A.10})$$

where  $I_{d_k^S}$  is the identity matrix of size  $d_k^S$ .

- **Consistency mass matrix  $M_C^E$ :**

Similarly to as for the consistency stiffness matrix we have

$$m^E(\pi_k^\partial(\phi_i); \pi_k^\partial(\phi_j)) = \int_E \pi_k^\partial(\phi_i) \pi_k^\partial(\phi_j) dx = \sum_{\alpha=1}^{r_k} \sum_{\beta=1}^{r_k} s_{\alpha,i}^\partial s_{\beta,j}^\partial m^E(m_\alpha; m_\beta),$$

therefore

$$M_C^E = (S^\partial)^T H^{(k,k)} S^\partial \quad (\text{A.11})$$

- **Stability mass matrix  $M_S^E$ :**

In this case the stability mass matrix is taken similarly as  $K_S^E$  with a proper scale:

$$s_m^E \left( (I - \pi_k^\partial) \phi_i; (I - \pi_k^\partial) \phi_j \right) = |E| \sum_{\ell=1}^{d_k^S} \text{dof}_\ell \left( (I - \pi_k^\partial) \phi_i \right) \text{dof}_\ell \left( (I - \pi_k^\partial) \phi_j \right),$$

where the factor  $|E| = \text{area}(E)$ , is imposed for scalability; therefore,

$$\boxed{M_S^E = |E| \left( I_{d_k^S} - S_\bullet^\partial \right)^T \left( I_{d_k^S} - S_\bullet^\partial \right)} \quad (\text{A.12})$$

We end this section stressing that all the contributions (A.9)–(A.12) are just computed once at the beginning of the simulation and as a result of the interpolatory approximation in the semi-discrete formulation (2.11a), no more expensive numerical integration of the nonlinear term at each time step is needed.